NASA Technical Memorandum 1999-209408

The Conductor-Dielectric Junctions in a Low Density Plasma

Boris Vayner, Joel Galofaro, Dale Ferguson, and Wim de Groot
John Glenn Research Center, Cleveland, Ohio 44135
Clint Thomson, J.R. Dennison, and Robert Davies
Utah State University, Logan, UT84322

Prepared for the
38th AIAA Aerospace Sciences Meeting and Exhibit,
Reno, Nevada, January 10-13, 2000

National Aeronautics and Space Administration

The Conductor-Dielectric Junctions in a Low Density Plasma

Boris Vayner[♣], Joel Galofaro[♠], Dale Ferguson[♠], Wim de Groot[♦],
Clint Thomson[$], J.R. Dennison[$], and Robert Davies[$]

Abstract. A conductor-dielectric junction exposed to the space environment is a frequent spacecraft design feature. Due to spacecraft charging and/or solar array operation, the conductor can acquire a high potential with respect to the surrounding plasma. If this potential is positive the insulators adjacent to exposed conductors can collect current as if they were conductors themselves. This phenomenon, called snapover, results in a substantial increase in current collection, and may even result in a glow discharge if the potential is high enough. If a conductor has a negative potential, arcing can occur at the site of a junction. Both of these phenomena negatively affect spacecraft operation. To prevent negative consequences, the physical mechanisms of snapover and arc inception require investigation.

In this paper, results are presented of an experimental and theoretical study of snapover, glow discharge, and arc phenomena for different materials immersed in argon or xenon plasmas. The effect of snapover is investigated for several metal-dielectric junctions: copper-teflon, copper-Kapton, copper-glass, aluminum-teflon, aluminum-Kapton, steel-teflon, anodized aluminum with pinholes, and copper-ceramics. I-V curves are measured and snapover inception voltages, essential parameters (increase in current and collection area due to secondary electrons), and glow discharge inception thresholds are determined. Optical spectra are obtained for glow discharges in both argon and xenon plasmas. These spectra provide information regarding atomic species entrapped in the glow region. Some spectral lines can be used to estimate plasma parameters in the discharge area. A video-camera and linear array were used to confirm that snapover inception is accompanied by very low intensity visible light emission. This result seems to be important for the estimate of the light pollution around spacecraft.

Optical spectra (wavelengths 380-650 nm) of arcs are also obtained on a negatively biased chromic acid anodized aluminum plate immersed in low density argon and xenon plasmas. Analysis of these spectra confirms our earlier findings that aluminum atoms are ejected from the arc site. Moreover, it is found that chromium atoms are also quite abundant in the arc plasma. It is believed that the latter results contribute considerably to the understanding of processes of plasma contamination caused by arcing.

[♣]Ohio Aerospace Institute, Cleveland, OH 44142
[♠]NASA Glenn Research Center, Cleveland, OH 44135
[♦]Dynacs Inc., Cleveland, OH 44135
[$]Utah State University, Logan, UT84322

1. Introduction.

A conductor-dielectric junction (CDJ), immersed in a plasma, demonstrates some interesting features when the conductor is biased positively or negatively with respect to the plasma. A sharp increase in the current collection can be observed with increasing bias voltage (snapover), as was found more than twenty years ago [1]. Since that time, much work has been done to understand the physical mechanism behind snapover, and to explain such observed features as the I-V curve and light emission from the area surrounding the conductor [2-5].

It is presumed that there are two physical reasons for the increase of the current collection, namely the generation of secondary electrons and the electrostatic discharge initiated in the small volume of dense gas due to outgassing. Distinguishing between these two causes is complicated by the fact that both mechanisms may occur simultaneously. In an effort to solve this problem, our procedure was to measure I-V curves repeatedly (usually ten times), and then to perform a statistical analysis of the measured parameters. If snapover is caused by secondary electrons, the inception voltage should be practically the same for all sweeps, for the chosen geometry and dielectric material, because the magnitude of the threshold voltage depends only on the first crossover voltage. Moreover, inception voltages are expected to be different for various dielectrics.

The realization of these ideas has resulted in the design of experimental samples that include different dielectrics (Kapton, teflon, ceramics, and anodized aluminum). In addition, in order to verify the hypothesis of secondary electron emission, conductors were installed with different diameters (0.6, 1.2, 2.5, and 5 cm), because the surface current depends on the conductor diameter. It is also believed that repeated biasing of the conductor to high voltages (up to 600 V), and long-time exposure of the sample to vacuum (pressure less than 1 μTorr), will cause outgassing of the CDJ. This idea was verified and confirmed during the experiments.

A subsequent step in the analysis of snapover was performed by recording the light emitted from the area around the conductor. The inception of glow was observed by the naked eye and video camera, and recorded on a VCR. Unfortunately, the intensity of the radiation was very low, and even though the rise of the signal was registered on a linear array, the spectral features of this radiation were too weak to detect. It should be noted that the image of the glow caused by the snapover was recorded and analyzed several years ago by implementing a special procedure for background subtraction [6].

When the bias voltage is increased above 500 V, a gas discharge can be observed in the vacuum chamber. The first indication of the discharge is a sharp increase in the collection current (sometimes up to the power supply limit of 10 mA). The second manifestation of the discharge is a bright ring around the conductor that could be seen by the naked eye and that is recorded by the VCR and linear array. Bright glows were observed in two plasmas; - argon and xenon. Spectra of the radiation were obtained in the wavelength range 380-500 nm. The identification of spectral lines confirmed the suggestion that the glow is caused by a gas discharge. Lines of argon and xenon were found but no lines of other species. One more argument in favor of a gas discharge is the known dependence of the threshold voltage to the neutral gas pressure. Here, the threshold voltage varies from 700 V to 1000 V with a pressure change from 300 μTorr to 200 μTorr in argon. The discharge in a xenon plasma initiated at lower pressures, 70-90 μTorr. All the above

considerations warrant the conclusion that the exposure of a positively biased CDJ to the space plasma can result in a sharp increase in the current collection, the generation of light pollution, and the initiation of a glow discharge around the site if the density of neutral gas around the spacecraft is high enough.

Another problem concerns negatively biased conductor-dielectric junctions. Any spacecraft powered by a solar array with a negative bus ground will acquire a negative potential with respect to the space plasma. At the same time, the surface of an adjacent dielectric will be charged close to the plasma potential. Thus, the potential drop between conductor and dielectric may almost reach the magnitude of the solar array operating voltage [7-8]. The situation is even worse for the spacecraft in GEO, where a spacecraft body may acquire a few kilovolts negative potential due to energetic electrons, and dielectric surfaces may be charged positively because of photoelectron emission caused by solar UV radiation. This differential charging may result in an electrostatic discharge-arc that is undesirable for spacecraft operation [9-11].

In this paper, we report a study regarding arcing on an aluminum anodized plate that simulates the body of a spacecraft. It was found that the arc threshold depends on the thickness of the anodized layer and the type of technological process used to manufacture the particular plate. In general, the threshold varies between minus 150 V and 300 V, but some samples demonstrate an even lower threshold (-80-100 V). Arcs on the surface destroy thermal insulation, leaving pinholes in the anodized layer. Several years ago it was shown that atoms of aluminum and other species, ejected into the plasma from the arc site, result in plasma contamination [12]. At that time, a mass-spectrometer was employed to analyze the composition of the ejected material. Aluminum atoms were identified, and the presence of unknown atoms with atomic mass A=52 was demonstrated. To confirm these earlier findings and to solve the puzzle with A=52 it was decided to perform optical spectroscopy of an arc plasma. Spectra were obtained in the wavelength range 380-650 nm, and spectral lines of aluminum and chromium (A=52) have been identified. This is peculiar because the presence of chromium in the arc plasma is the result of the processing technology during anodized aluminum production, namely anodizing in chromic acid bath.

To measure spectra within the whole range of wavelengths, tens of arcs have been initiated. These arcs left a similar number of pinholes in the anodized layer that provided the possibility to study snapover and glow discharge on the flat surface where these CDJs are scattered randomly. The measurement of I-V curves confirmed the inception of snapover. However, in this case an exponential increase in the current collection was observed that differs substantially from the I-V curve measured for a single conductor-dielectric junction. A subsequent step in the experimentation with the aluminum plate was the analysis of a glow discharge inception and matching spectrum, after the plate was biased positively to a high voltage (up to 600 V). Spectral lines of argon and xenon, which are expected for such a discharge, were identified. The inception of weak light emission was also observed at low voltages (150-200 V) but no spectra were measured due to the low intensity. Unexpectedly, it was found that biasing the aluminum anodized plate to a positive 350-400 V resulted in the destruction of the anodized layer. Contamination of the surrounding plasma due to this effect was anticipated, but no spectral lines of any other elements besides argon and xenon were found. This fact may be explained by the big differences in line intensity of these gases, as compared to

spectral lines of other species, which make it impossible to identify weak lines by using a low resolution spectrometer.

It was shown that with the use of relatively simple equipment, software, and experimental methods, a successful determination of the chemical composition of the discharge plasma in the case of arcing on an aluminum anodized plate was possible. Future work is intended to employ more elaborate methods to answer some questions regarding the inception of arcs on the solar array. But these issues are beyond the scope of the current paper.

2. **Experimental Setup.**

All experiments were performed in the 1.8 m. diameter, 3 m long vacuum chamber installed in the Plasma Interaction Facility (PIF) at NASA's Glenn Research Center (GRC) [13]. In this facility, ambient pressure as low as 10^{-7} Torr can be achieved. Two Penning sources were installed to generate argon or xenon plasma with an electron density of $n_e=(0.1\text{-}10)\cdot10^5$ cm^{-3}, a temperature of $T_e=1\text{-}2.5$ eV, and a neutral gas pressure of $p=(0.7\text{-}\ 7)\cdot10^{-5}$ Torr, which could be kept steady during an experiment. A set of twenty samples was vertically mounted in the middle of the chamber. Each sample could be biased to the power supply provided voltage, from 0 to 1 kV, positive or negative (Fig. 1). Each sample was assembled as a 10x10 cm teflon plate with a metallic cylinder in the middle. The back sides of all conductors were insulated. Three left top panels were covered with Kapton strips. Only one steel hemisphere was tested.

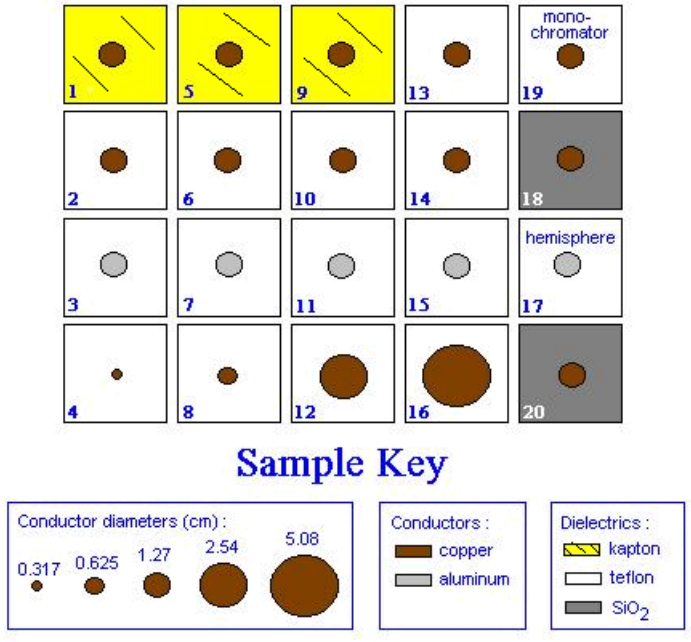

Fig. 1. Layout of conductor-dielectric simulations

Diagnostic equipment included one spherical Langmuir probe with a diameter d=2 cm, one wire probe, one linear array equipped with optical spectrometer, one video camera with VCR, one current probe with an amplifier to measure arc current, two oscilloscopes to control signals triggering a pulse generator which electronically opens a linear array gate, and two PCs to collect and analyze data (see details in Ref. 14). To simulate spacecraft capacitance, an additional capacitor C=1-2 μF was installed between the aluminum plate and ground in the experimental series with the anodized aluminum plate. The optical system consisted of a medium fast collection lens, a spectrometer, a linear array, and a PC, used to measure and analyze spectra in the wavelength range 380-650 nm. This equipment and software were successfully used to determine the chemical composition of the discharge plasma in the case of arcing and the glow on the aluminum anodized plate, and glow discharge on one sample (No.19 in Fig. 1).

3. Snapover

To obtain I-V curves for each sample, the conductor was increasingly biased (swept) from –100 V to +600 V and backward in 5V steps, with a step time of 0.5 s. But before turning to the analysis of the I-V curves, the sample potential with respect to the plasma needs to be calculated. The power supply indicates the voltage with respect to the chamber wall, which is grounded (zero potential). The plasma potential, measured by sweeping a Langmuir probe is approximately 15 V. To determine the relaxation time for a sample, the following sequence of measurements was employed: a) the sample is initially biased to zero volts (slightly negative with respect to the plasma); b) the power supply is switched to a few hundred volts. The results of the current measurements are shown in Fig.2.

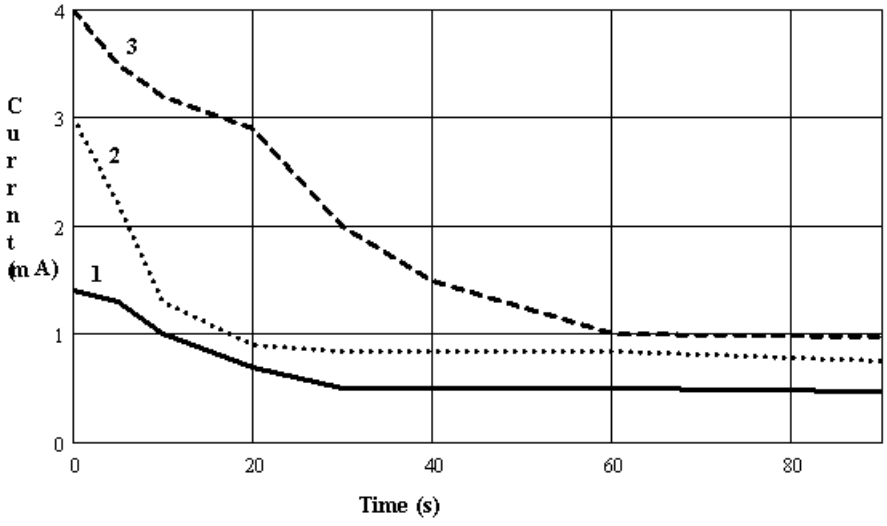

Fig.2. Collection current vs. time for three initial bias voltages: 1-500V; 2-600V; 3-700 V.

The relaxation times determined from these three curves are rather widely scattered, but an average value of 15-30 s may be adopted for further analysis. If the sample is simulated as a capacitor that is charging through the resistor (plasma), the equation for the conductor potential could be written as follows:

$$U_c(t) = \frac{\alpha}{\tau} \cdot \exp\left(-\frac{t}{\tau}\right) \cdot \int_0^t x \cdot \exp\left(\frac{x}{\tau}\right) \cdot dx \qquad (1)$$

where α is the voltage change rate (usually 10V/s), and τ is the relaxation time.

Fig.3 shows that the sample potential is always lower than the bias voltage. This result is important for further analysis of the snapover inception. It should be stressed that the plasma potential does not change the results of the analysis because the critical voltage is much higher than the voltage drop between plasma and ground.

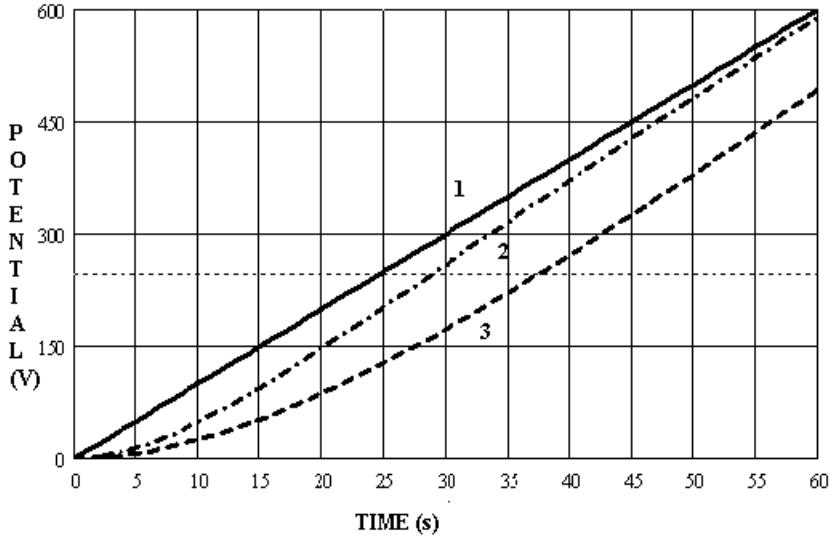

Fig.3. The sample potential vs. time for two different relaxation times. 1) bias voltage; 2) τ=15 s; 3) τ=30 s.

In order to perform tests for many different samples, and to collect representative statistics, the time of each sweep was decreased. That is why some measurements were done with a rate of 20 V/s that caused the gap between bias voltage and sample potential to be substantially higher. However, to test the snapover inception more accurately, a few samples were swept with the rate of 1 V/s. In this case there was almost no difference between the bias voltage and the sample potential. One example of I-V curve measurements for a particular sample (1.27 cm copper – teflon junction) is shown in Fig. 4. This figure illustrates that the snapover inception threshold is approximately equal up to 300 V (289±47 V for ten sweeps). Fluctuations in the threshold magnitude could be explained by changes in plasma parameters during the measurements, which take about sixty minutes for ten sweeps to complete, and by the contamination of the dielectric surface around the conductor. However, the sharp increase (jump) in current was observed for all

samples (except for the aluminum plate which will be discussed below). This observation allows the identification of the cause of this jump as being the generation of secondary electrons on the dielectric surface. One more argument in favor of the secondary electron generation argument is the change in the slope of the I-V curve. From the moment that the secondary electron yield exceeds one, the collection current is caused mainly by the surface current. An important issue in distinguishing between the two hypotheses of snapover inception mechanism - secondary electrons or gas discharge - is the correlation between a threshold voltage (measured) and the 'first crossover' potential. According to Ref. 15, the maximum secondary electron yield is Y_m =2.12, where the electron beam energy for this yield is E_m =400 eV for teflon. If a simple double-exponent approximation [16] for the function $Y(E)$ is applied, the first crossover energy can be estimated as $E_1 = 100$ V.

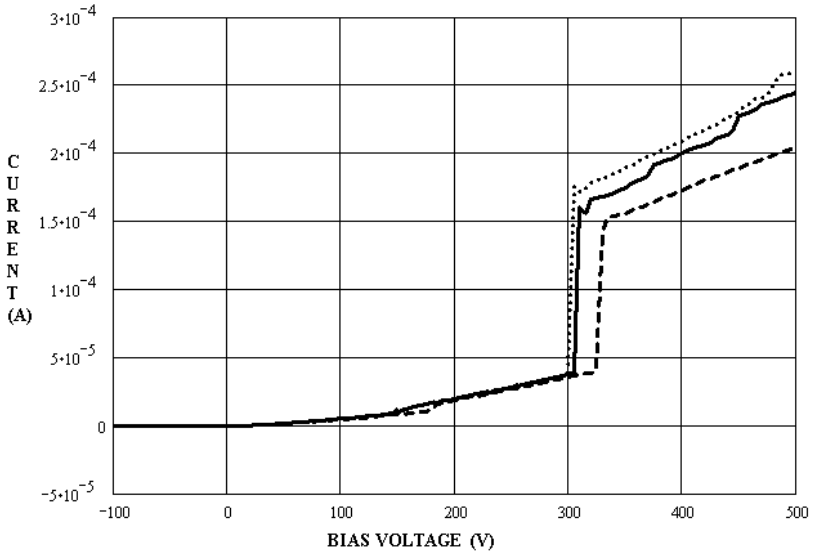

Fig.4. Three examples of I-V curves that demonstrate the snapover inception. The change in slope is clearly noticeable. (α=10 V/s)

This estimate is in agreement with the measurements for the 30 s relaxation time (see Fig. 3). Several measurements have been done with a 2.5 V/s rate (Fig.5). The snapover inception voltage here decreases considerably, as is expected. In reality, the situation is increasingly complicated as the result of the unknown distribution of potential along the dielectric surface, the out of normal incidence of primary electrons, the probable presence of an oxide layer with high Y_m, and the unknown degree of surface contamination. Before turning to the data analysis, results are shown of measurements for different combinations of conductor - dielectric materials, conductor sizes and shapes (Table 1). The results shown in Table 1 are obtained in an argon plasma. All measurements have been repeated in a xenon plasma with substantially the same results, which leads us to believe that the ion mass does not play an essential role in the physical mechanism of snapover. The difference in I-V curves measured in argon and xenon plasmas appeared at

much higher voltages, at a level where the gas discharge initiation becomes possible. It follows from the data that the dependency of inception voltage on dielectric material and conductor size is rather weak. Even though the magnitudes of the inception voltage scatter widely, the difference between row #9 in Table 1 and the other rows is obvious. This difference is attributed to a zero relaxation time

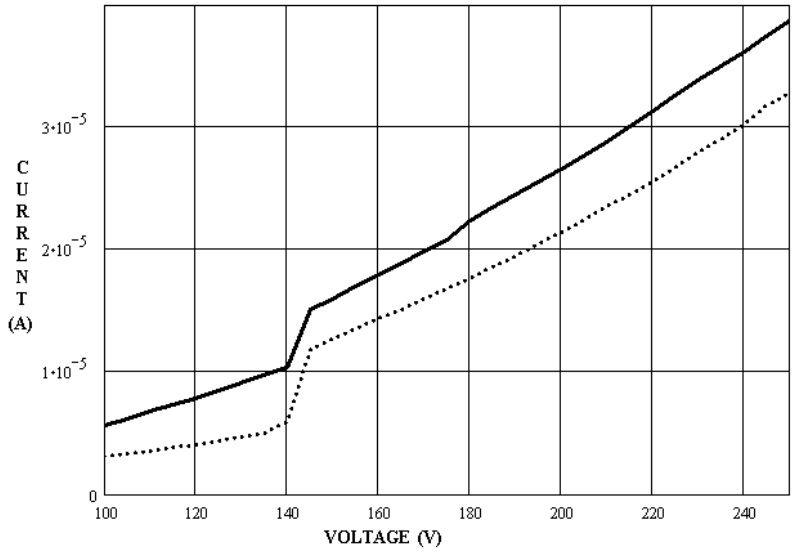

Fig.5. The snapover inception voltage shifts to the lower magnitude with a decreasing sweep rate. Two I-V curves are shown for α=2.5 V/s.

Exp. No	Conductor	Diam (cm)	Dielectric	Inception Voltage (V)	Current ratio	Increase in I-V curve slope
1	copper	1.27	teflon	289(47)	4.6(1.23)	2.34(0.52)
2	copper	1.27	Kapton	279(25)	3.18(0.87)	2.88(1.27)
3	steel	1.27	teflon	268(12.6)	4.7(1.6)	2.95(0.95)
4	aluminum	1.27	teflon	243(6)	4.5(0.17)	3.4(0.7)
5	copper	0.32	teflon	230(23)	47(16)	43.8(13.6)
6	copper	0.64	teflon	316(51)	29(21)	21.7(16)
7	copper	2.54	teflon	198(6)	3.25(1.0)	2.18(0.63)
8	copper	5.1	teflon	211(14)	1.96(0.33)	1.91(0.33)
9	copper	0.02	ceramic	155(3.5)	4.2(0.3)	3.66(0.75)
10	copper	1.27	glass	235(9.6)	3.3(0.6)	5.1(0.7)

Table 1. Snapover inception voltages and characteristics of I-V curves for different CDJs. All results were obtained in argon plasma with an electron number density $n_e=3.3\cdot10^5$ cm^{-3}, electron temperature T_e=2.2 eV, and argon pressure 73 μTorr. Standard deviations are shown within parenthesis.

for the last sample which is a simple coax feed-through. The dependence of the current ratio on the conductor diameter is far more obvious (Fig. 6).

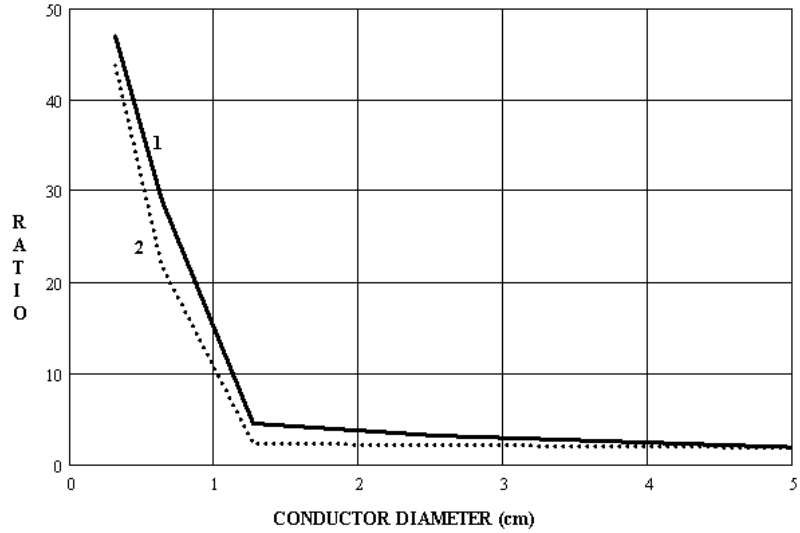

Fig.6. The current ratio (1) and the slope increase (2) vs. conductor diameter (copper on teflon).

A possible explanation for the dependence of the I-V curve parameters on the conductor diameter can be found in the different ratio between the Debye length and the size of conductor. The Debye length for the plasma parameters shown above is approximately 2 cm. When the conductor diameter is much less than this length the current collection can be described in the orbit-limited approximation. For a larger conductor diameter, the thin sheath approximation should be applied. The difference in these theoretical models may explain the different behavior of I-V curves at voltages below the snapover inception voltage. To explain the big difference in current ratios and the slopes, one needs to consider the current collection due to surface conductivity induced by secondary electrons.

4.Theoretical model.

One of the principle parameters describing the current collection in a plasma is the thermal current density:

$$j_T = e \cdot n_e \cdot \int_0^{\infty} v_z dv_z \cdot \int_{-\infty}^{\infty} f(v_x, v_y, v_z) dv_x dv_y \qquad (2)$$

where $f(v)$ is the electron distribution function.

If it is assumed that this distribution function is Maxwellian, the current density can be expressed as a function of two variables only:

$$j_T(n_e, T_e) = e \cdot n_e \cdot \left(\frac{T_e}{2\pi m_e} \right)^{1/2} \qquad (3)$$

For a plasma with parameters $n_e = 3 \cdot 10^5\, cm^{-3}$ and $T_e = 2\ \ eV$, the thermal current density equals 1.6 μA/cm^2. According to the planar probe theory, the current should not depend on the bias voltage (when $U >> U_{pl}$) [17]. In reality, nonzero slopes of I-V curves were measured for all samples. The measured value of *dI/dV* increases approximately linearly with the sample area. However, if the orbit-limited current approximation is applied, then

$$I(U) = j_T \cdot S \cdot (1 + \frac{U}{T_e}) \qquad (4)$$

where the calculated current and slope exceed the measured values almost an order of magnitude for large samples. It is generally accepted that the orbit-limited current approximation works better, when the size of the probe is much less that the Debye length λ_D. For the current experiments, the measured slope is 0.05 μA/V for the sample with a *0.32* cm diameter (theoretical value 0.06 μA/V), and 1 μA/V for *5* cm diameter (theoretical value 16 μA/V). That is why two different areas are considered in Fig.6: $d<2$ cm and $d>2$cm. To compare experimental results with theoretical predictions of the I-V curve parameters, it is necessary to calculate the surface current carried by the secondary electrons. The distribution function of the SE can be represented as

$$F(E, \Theta) = A \cdot F(E) \cdot \cos^{\beta} \Theta \qquad (5)$$

where E is the energy of electrons, A and β are constants, and Θ is angle between the electron velocity and the normal to the surface.

The normal component of the secondary electron current density vector can be written in the following form:

$$j_s = n_s \cdot e \cdot \bar{v} \cdot \frac{\beta + 1}{\beta + 2} \qquad (6)$$

where $n_s(E) = \int_0^{\infty} F(E)dE$ is the number density of secondary electrons, $\bar{v} = \int_0^{\infty} \left(\frac{2E}{m_e} \right)^{1/2} F(E)dE$ is the average electron speed, and β is believed to be close to 1 [16].

The ratio of the secondary electron number density to the plasma electron number density can be obtained by combining Eqs. 3, 4 and 6

$$\frac{n_s}{n_e} = Y \cdot \left(\frac{T_e}{4\pi W} \right)^{1/2} \cdot \left(1 + \frac{U}{T_e} \right)^{-1} \cdot \frac{\beta + 1}{\beta + 2}$$

where $W = \int_0^\infty E \cdot F(E) dE$ is the average initial energy of secondary electrons (usually 5-10 eV).

When the bias potential is low (zero), the dielectric surface will charge negatively due to the higher electron mobility. During a sweep, the bias voltage increases which results in the increase of flux and electron energy. At some bias voltage magnitude U_1, the average electron energy becomes equal to the first crossover energy W_c. From that moment, even a small rise of the bias voltage causes the generation of secondary electrons with a yield $Y>1$, and the dielectric surface acquires a positive surface charge. The normal component of the electrical field strength can be found from the equation:

$$E_n = \frac{\sigma_+}{2\varepsilon_0} \qquad (7)$$

where $\varepsilon_0 = 8.85 \cdot 10^{-12}$ F/m is the dielectric constant, and σ_+ is the surface charge density.

The electrical field strength vector parallel to the insulator surface, E_t, is proportional to the gradient of the electrostatic potential that has been generated by biasing the conductor. The secondary electron emitted with the initial energy W will be hopping toward the electrode along the parabolic trajectory with the height

$$Z_m = \frac{W}{eE_n} \cdot \cos^2\theta \qquad (8)$$

The flow of these electrons that reach the electrode has to be considered as a surface current I_s. If the surface density of hopping electrons is σ_- then the surface current density can be written as

$$j_t = \sigma_- \cdot V_e \ \text{(A/m)} \qquad (9)$$

where V_e is the average velocity parallel to the surface of the dielectric.

As was shown in Ref. 18, the avalanche of secondary electrons is auto regulating in such a way that the average energy at impact should be equal to the first crossover energy W_c. If the increase of E_n on the length of one hop is disregarded, the average velocity can be calculated as:

$$V_e = 0.5 \cdot \left(\frac{2W_c}{m_e} \right)^{1/2} \qquad (10)$$

and the electrical field strength is:

$$E_t = E_n \cdot \left(\frac{W_c - W}{2W} \right)^{1/2} \qquad (11)$$

If we assume that $\sigma_- = a \cdot \sigma_+$ ($a \leq 1$ is a numerical factor), and substitute Eqs. (7),(10), and (11) into Eq. (9), the surface current density can be written as:

$$j_t = a\varepsilon_0 \cdot \left(\frac{2W}{W_c - W}\right)^{1/2} \left(\frac{2W_c}{m_e}\right)^{1/2} \cdot E_t \qquad (12)$$

The net current measured at voltages $U>U_1$ can be represented by the sum of plasma current $I(U)$ and surface current $I_s = \pi d j_t$. The increase of current collection δ at voltage U_1 (Table 1) can be calculated for two different situations: $d<\lambda_D$ and $d> \lambda_D$. In the first case we may substitute Eq.4 into Eq. 12 to obtain the following result:

$$\delta = 1 + 8\frac{a \cdot \varepsilon_0 \cdot T_e}{d \cdot W_c \cdot j_T} \cdot \left(\frac{2W}{W_c - W}\right)^{1/2} \cdot \left(\frac{2W_c}{m_e}\right)^{1/2} \cdot E_t \qquad (13)$$

It is worth noting that the current increase is inversely proportional to the sample diameter for $d<\lambda_D$, for which case the theoretical formula is in a good agreement with measurements. To find the numerical value of δ, it is necessary to estimate the field E_t. If it is assumed that the height of the electron trajectory should be less than the Debye length

$\frac{W}{E_n} < \lambda_D$ (not to allow the secondary electron returning in the background plasma) , and if Eq.11 is substituted in this inequality, the following results can be obtained from Eq.13: $\delta(0.32)= 42$ and $\delta(0.64)=21.5$ (for $a=1$). The last two numbers are in very good agreement with experimental data (see Table 1). With increasing sample diameter, the process of current collection becomes more complicated, and the dependence $\delta(d)$ weakens compared with Eq.13. In this case, a computer simulation is needed to get a quantitative agreement between theory and experiment (see Ref. 19).

One more argument in favor of secondary electron emission should be added as a physical reason for snapover. When the dielectric surface near the conductor was covered with a carbon powder, the jump in the I-V curve vanished.

5.Glow.

The maximum voltage increase during a sweep was accompanied by the observation of several other physical events. First of all, a glow discharge was observed by the naked eye, and subsequently registered with a video camera (Fig. 7). First, the inception of the discharge changes the visible image from a very weak and diffuse white light to quite a powerful violet glow around the central conductor. Second, a sharp current increase is registered simultaneous with the inception of the glow (Fig.8).

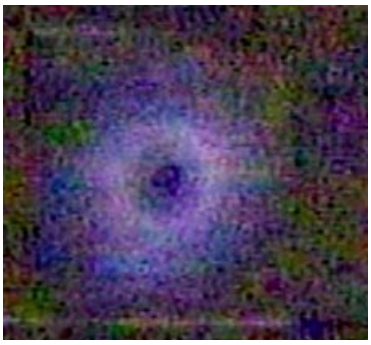

Fig.7. A glow discharge has been observed in an argon plasma with a pressure of $3*10^{-4}$ Torr. The sample is a 1.27 cm copper cylinder inserted in a teflon plate.

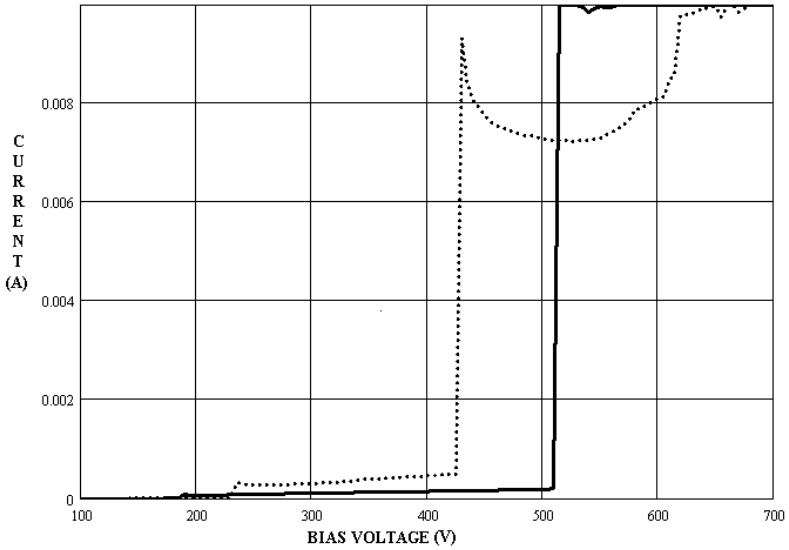

Fig.8. Two I-V curves are shown for the experiments for which glow discharges have been observed. The initiation voltage varies from 420 V to 510V. Cutoff at the 10 mA current is caused by the power supply limitation (Top of graph).

The current increase at 230 V, barely noticeable, is caused by real snapover. As mentioned above, snapover is accompanied with a weak optical emission. If the voltage (and current) continues to rise, the initiation of a glow discharge becomes highly probable. The neutral gas pressure, however, should be kept well above the usual upper limit in order to initiate this discharge at voltages below 1 kV. Due to the particular experimental setup, the glow was sustained for 20-30 s in order to obtain spectra in both argon and xenon plasmas. Two examples of spectra are shown in Fig.9.

The experimental arrangement used to obtain the spectra consists of a collection lens, a refocusing lens, a 0.15 m spectrometer, and an intensified 700 pixel array. Even though the 1200 groove/mm equipped spectrometer provides relatively poor resolution, excellent qualitative spectra can be obtained. Using a narrow, 50 μm, slit allows an acceptable resolution. The linear array was a red-enhanced diode array of 1024 pixels, of which 700 channels were active. A pulsed gate allowed spectra to be obtained with exposures from

a several nanoseconds to milliseconds duration. The spectrometer/intensified array assembly was calibrated within the wide range of wavelengths (380-650 nm) with a standard argon lamp (Oriel 6030), a neon lamp (Oriel 6032), and a helium-neon laser

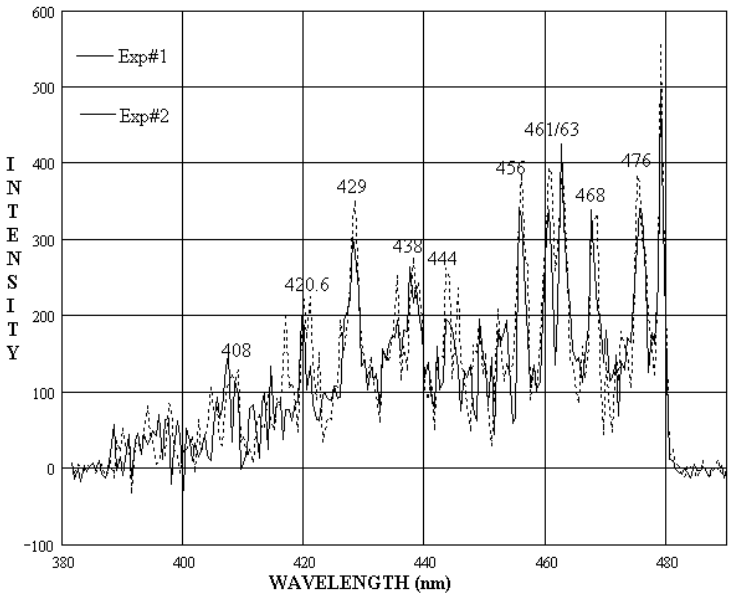

a)

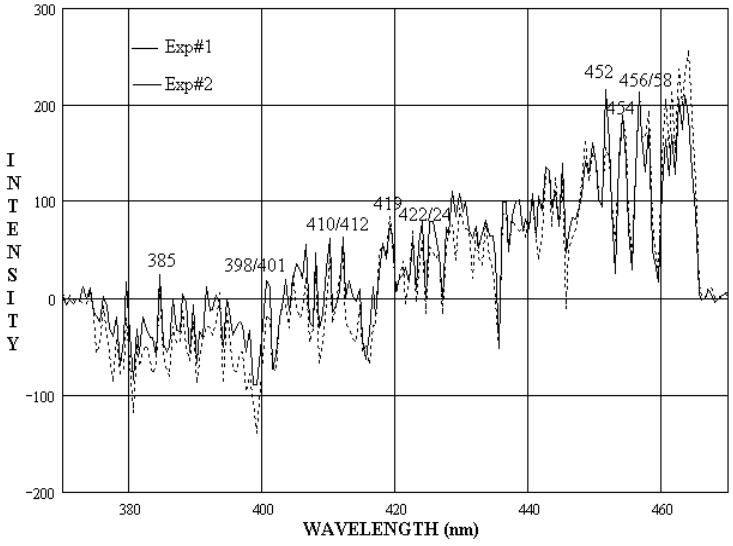

b)

Fig.9. Examples of spectra of glow in (a) argon and (b) xenon plasmas. Only spectral lines of background gases have been identified. Two measurements are shown on each plot.

(632.8 nm). A linear relation between array pixels and wavelengths was used for all ranges. However, the slope and the central wavelength were determined for each range

separately. The conversion of pixels in nanometers has been done according to the following formula:

$$\lambda(p)=\lambda_0-k(p-b) \qquad (14)$$

where λ_0 is the wavelength of a calibration line, b is the corresponding pixel number, and k is the slope determined usually by using two-three calibration lines for each wavelength range.

It should be noted that some deviation was observed from the linear relation near the edges of working range (pixels 200-300 and 800-900), but multiple measurements within the overlapped wavelength intervals have provided quite reliable determinations of atomic spectral lines.
As it follows from the Eq.(14) the error in the determination of wavelength caused by error in the slope k can be found from the relation:

$$\frac{\delta\lambda}{\lambda}=\frac{\lambda-\lambda_0}{\lambda}\cdot\frac{\delta k}{k} \qquad (15)$$

Statistical analysis of calibration data has resulted in the determination of standard deviation for $\delta k/k$: $\Delta=0.02$. Thus, this methodology allowed the error in the

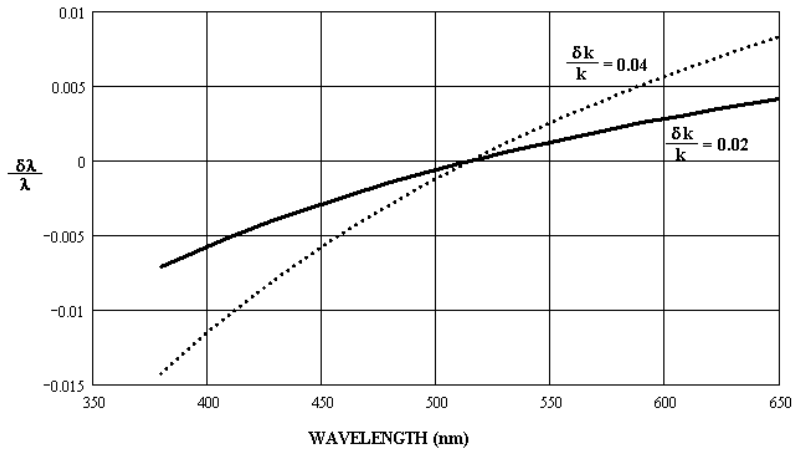

Fig.10. The error in the determination of the wavelengths of spectral lines does not exceed 1% within the entire range of wavelengths.

determination of spectral lines not to exceed 1% (Fig. 10).

After all measurements were done, the results were compared with data compiled in Ref. 20. Even though some lines (414 nm in argon and 412/415 nm in xenon) were found that might belong to other species, no identifications were made besides these background gases.

6. Arcing and glow on an aluminum anodized plate.

Anodized aluminum has been used in the construction of spacecraft for many years. Long ago it was found that electrostatic breakdown (arc) of the anodized layer is possible if the metal is charged less than negative one hundred volts with respect to the surrounding plasma [21]. Extensive ground testing demonstrated that arcs are damaging to anodized layers, and that material ejected from the arc site contaminates the spacecraft environment [12]. An electrostatic discharge generates a pulse of light. The spectrum of this optical emission can provide information about the chemical composition of arc plasmas. To the authors' knowledge, the first measurements of such spectra were obtained five years ago for arcs initiated on the interconnect of a solar array sample [22]. Two spectral lines were identified, both of them belonging to silver, and originating from the interconnect, which is Ag-plated. Previously, a quadruple mass-spectrometer was used to determine the plasma contamination due to arcing on anodized aluminum. It was shown that the number density of aluminum atoms in the plasma chamber increased considerably. Moreover, an increase in number density of other species, particularly with atomic mass A=52 was detected, but the origin of this element was not identified at that time [12]. Therefore, a spectral analysis of the arc plasma is a logical continuation of previous work devoted to the study of arcing in low density plasmas.

For this particular experiment a 10x10 cm aluminum anodized plate was installed in front of a quartz vacuum tank window. To avoid possible tank wall effects on the potential distribution, the distance between plate and tank wall was chosen to equal 40 cm. The back side and edges of the plate were insulated with Kapton strips. The plate was biased negatively (usually minus 300 -350 V) through a 10 kOhm resistor with an additional 2 μF capacitor installed between the plate and ground. When arcing occurs, the discharge current pulse triggers a pulse generator which opens the electronic linear array gate for 100 μs. The light collected was focused on the slit of the spectrometer by a short (4 cm) focal lens creating fast optics with an f# of 4. Spectra were obtained of arcs in both argon and xenon plasmas within the range of wavelengths 380-650 nm. Examples of spectra are shown in Fig.11. Two distinct lines were identified for each spectrum, at 394.4, and 396.1 nm, corresponding to known aluminum lines.

According to the NIST Atomic Spectra Database [23] these two lines correspond to the dipole transition $3s^2\left(^1S\right)4s - 3s^2\left(^1S\right)3p$ ($J_1=1/2$, $J_2=3/2$). Unfortunately, no strong aluminum lines exist with wavelengths between 400nm and 650 nm. But several lines (469.8, 520.8, 659.4, and 688.3 nm) were observed that are believed to belong to chromium (Cr I) atoms. One sample spectrum is shown in Fig.12.

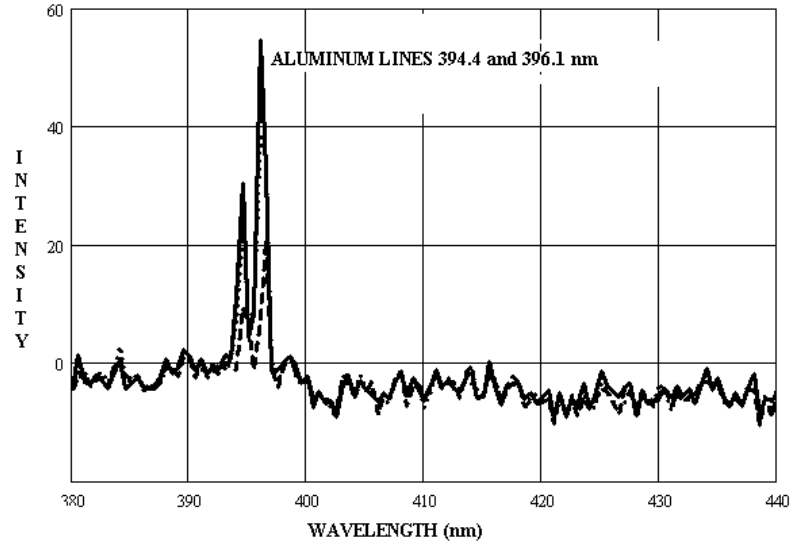

a)

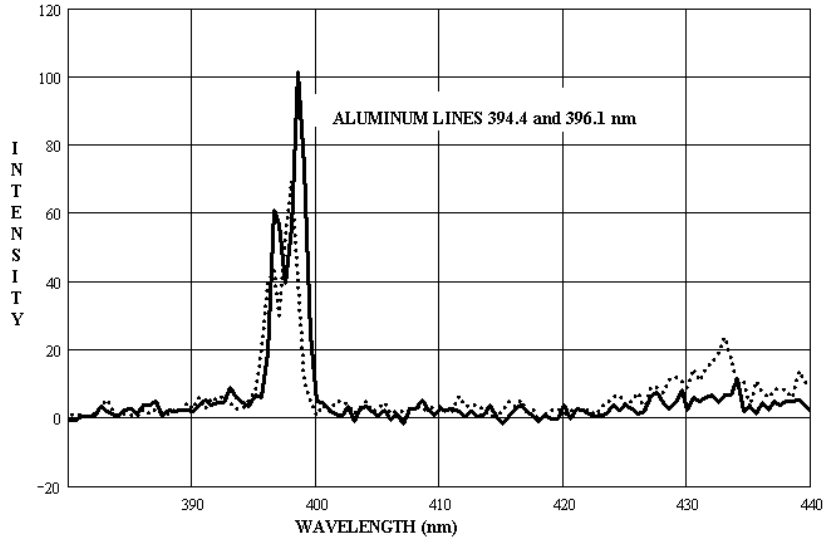

b)

Fig.11. Low resolution spectra of arc plasmas in argon (a) and xenon (b). Aluminum (Al I) lines are identified in both background gases.

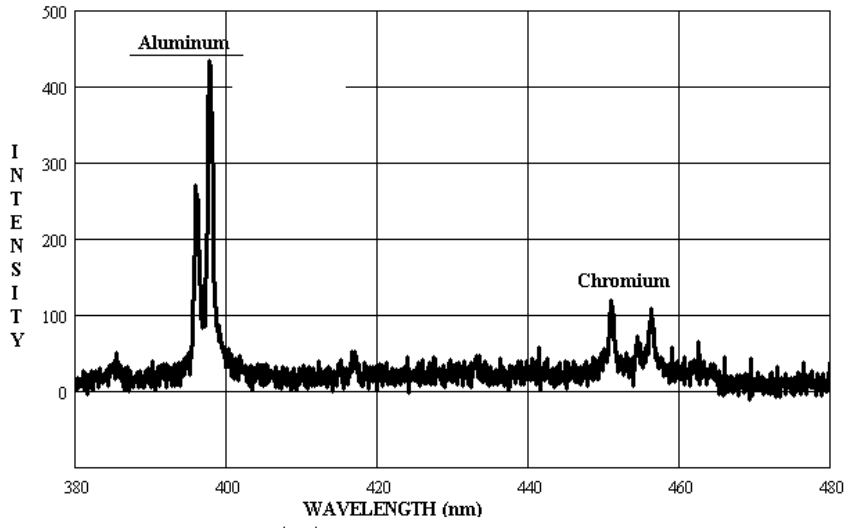

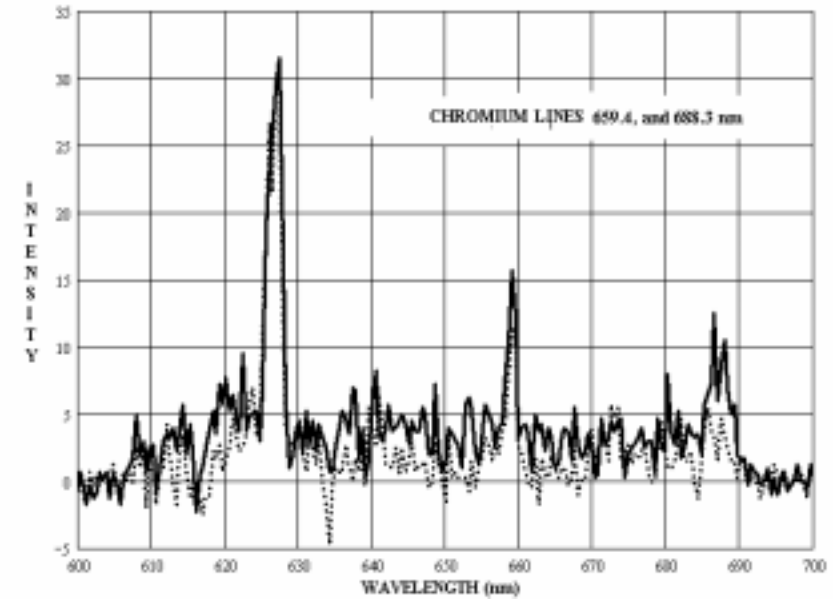

Fig.12. Several spectral lines of chromium (Cr I) are identified. The intensity of these lines is 2-4 times lower than the intensity of aluminum spectral lines. The line 626 nm is not identified.

The presence of chromium atoms in the arc plasma is caused by the production methodology of anodized aluminum. According to specifications [24], the coating is produced by anodizing in a chromic acid bath. The identification of chromium confirms the earlier identification of an element with atomic mass A=52 in the arc plasma. It is

believed that these results can be useful for the analysis of spacecraft environmental contamination caused by arcing on its surfaces.

Arc spectra measurements left approximately one hundred pinholes in the anodized layer. This provided the opportunity to investigate snapover on the aluminum anodized plate. The sample was biased three times from 0 to 600V. The resulting I-V curves are shown in Fig.13. Snapover inception was confirmed at about 100 V, but the I-V curve character appeared to be different from I-V curve shown in Fig.4. The current grows exponentially with the bias voltage but no jump in the I-V curve occurs. This is attributed to the difference in geometrical features of the latter experiments, namely the multiple pinholes distributed randomly over a large surface. A glow discharge initiation is observed at 530-550 V. The spectrum of this discharge consists of spectral lines of background gases (xenon lines for the particular data shown in Fig.14). It should be noted that biasing the plate positively above 400 V resulted in a fracture of the anodized layer. Many black spots can be seen with the naked eye, and the current collection increases as the result of the destroyed insulator (see Fig.13). This result seems important for LEO spacecraft design.

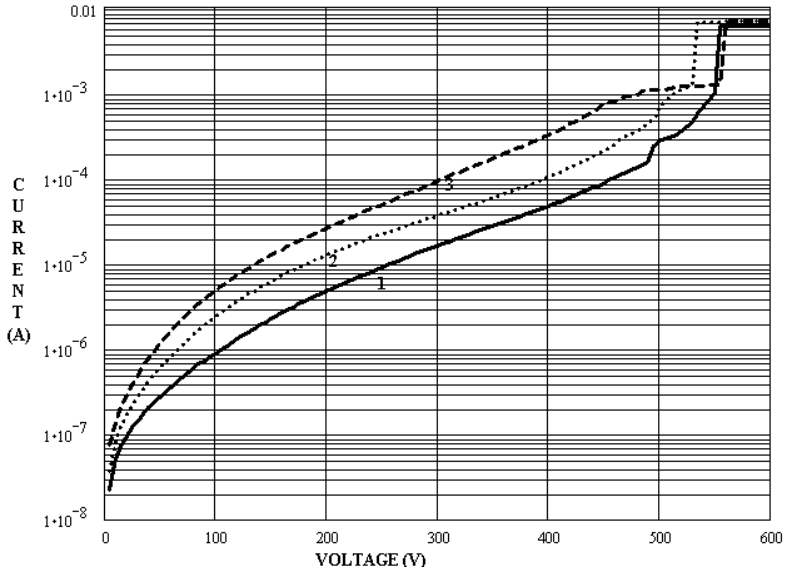

Fig.13. Three I-V curves, measured for the anodized aluminum plate. The snapover initiation is clearly visible at voltages just above 100 V. The inception of a glow discharge at 530-550 V results in the sharp current increase. Numbers 1, 2, and 3 indicate the measurement sequence.

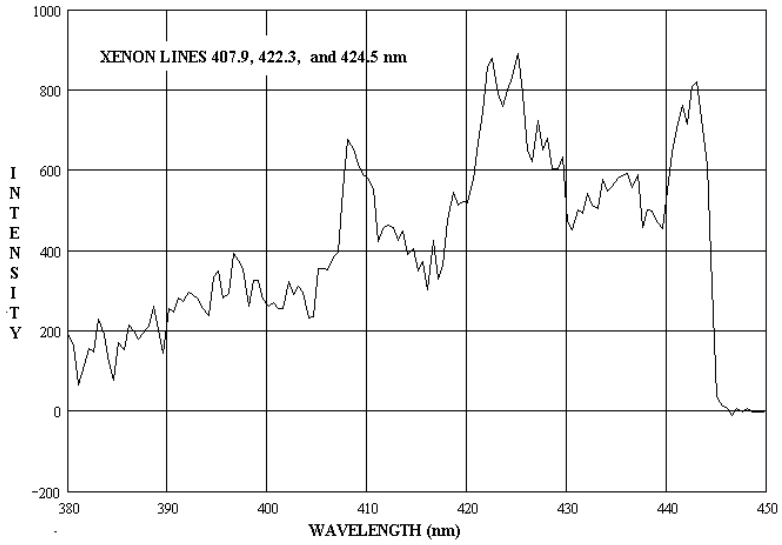

Fig.14. Example low-resolution spectrum of glow discharge on aluminum anodized plate immersed in a xenon plasma. A wide slit (100 μm) was used for this particular measurement.

Conclusion.

Comprehensive tests of conductor-dielectric junction immersed in low-density plasmas have shown that a sharp increase of current collection (snapover) is caused by the emission of secondary electrons. This increase can be over an order of magnitude. Thus, it is important to take this effect into account when designing solar arrays with exposed interconnects, or any other elements of the spacecraft that include a conductor-dielectric junction exposed to the space plasma. In addition, a weak optical emission emanating from the dielectric plate is observed when the conductor is biased above the snapover inception voltage. This observation is considered important for the analysis of light pollution around spacecraft. At the same time, a bright glow discharge can be initiated at high voltages and high neutral gas densities that appear to be unrealistic for real spacecraft. Earlier findings were confirmed that arcs on a negatively biased aluminum anodized plate emit aluminum and chromium atoms in the surrounding plasma, which can result in adverse consequences, i.e. contamination of sensitive spacecraft surfaces. It was demonstrated that snapover on an aluminum anodized plate results in the destruction of the thin anodized layer, which in return can influence the spacecraft thermal control. All these results contribute considerably to our understanding of the spacecraft-environment interaction.

References

1. Grier, N.T., and Dominitz, S. “Current From a Dilute Plasma Measured Through Holes in Insulators”, NASA TN-D-8111, December 1975
2. Katz, I., Mandell, M.J., Schnulle, G.W., Parks,D.E., and Steen, P.G. “Plasma Collection by High-Voltage Spacecraft at Low Earth Orbit”, Journal of Spacecraft and Rockets, 1981, Vol.18, No.1, p.79.
3. Carruth Jr, M.R. “Plasma Collection Through Biased Slits in a Dielectric”, Journal of Spacecraft and Rockets, 1987, Vol.24, No.1, p.79.
4. Davis,V., and Gardner, B. “Parasitic Current Collection by Solar Cells in LEO”, AIAA Paper 95-0594, 1995.
5. Hillard, G.B. “Plasma Chamber Testing of Advanced Photovoltaic Solar Array Coupons”, Journal of Spacecraft and Rockets, 1993, Vol.31, No.3, p. 530-532.
6. Ferguson, D., Hillard, G., Snyder, D., and Grier, N. “The Inception of Snapover on Solar Arrays: a Visualization Technique”, AIAA Paper 98-1045, 1998.
7. Stevens, N.J. “Interactions Between Spacecraft and the Charge-Particle Environment”, Proc. Spacecraft Charging Technology Conference, 1978, NASA CP-2071, p.268-294.
8. Hastings, D.E. “A Review of Plasma Interactions With Spacecraft in Low Earth Orbit”, Journal of Geophys. Research, 1995, Vol.100, No.A8, p.14,457-14,483.
9. Ferguson, D.C. “Solar Array Arcing in Plasmas”, Proc. 3rd Annual Workshop on Space Operations, Automation, and Robotics, Houston, Texas, July 25-27, 1989.
10. de la Cruz, C.P., Hastings, D.E., Ferguson, D.C., and Hillard, D.B. “Data Analysis and Model Comparison for Solar Array Module Plasma Interactions Experiment”, Journal of Spacecraft and Rockets, 1996, Vol. 33, No.3, p.438-446.
11. Galofaro, J.T., Doreswamy, C.V., Vayner, B.V., Snyder, D.B., and Ferguson, D.C. “Electrical Breakdown of Anodized Structures in a Low Earth Orbital Environment”, NASA TM 209044, April 1999.
12. Vayner, B.V., Doreswamy, C.V., Ferguson, D.C., Galofaro, J.T., and Snyder, D.B. “Arcing on Aluminum Anodized Plates Immersed in Low-Density Plasmas”, Journal of Spacecraft and Rockets, 1998, Vol.35, No.6, p.805-811.
13. Ferguson, D.C. “The Role of Space Plasma Simulation Chambers in Spacecraft Design and Testing”, NASA Lewis Research Center Report 96380, Feb. 1996.
14. Galofaro, J.T., Vayner, B.V., de Groot, W.A., and Ferguson, D.C. “Inception of Snapover and Gas Induced Glow Discharges”, Proc. 38th AIAA Aerospace Sciences Meeting and Exhibit, January 10-13, 2000, Reno, Nevada.
15. Krauss, A.R. “Localized Plasma Sheath Model of Dielectric Discharge of Spacecraft Polymers”, Final Report AFWL TR-88-37, February 1989.

16. Beyst, B., Rezvani, A., Young, B., and Friauf, R.J. “Procedures for Including Secondary Electron Emission in Numerical Simulations of Plasma-Insulator Interactions”, NASA CR 187090, March 1991.

17. Hershkovitz, N. “How Langmuir Probes Work”, in: Plasma Diagnostics, Vol.1, Eds. O.Auciello, and D.L. Flamm, Academic Press, Inc., San Diego, CA 1989, p.130-134.

18. Pillai, A.S., and Hackam, R. “Surface Flashover of Solid Dielectric in Vacuum”, Journal of Applied Physics, 1982, Vol.53, No.4, p.2983-2987.

19. Mandell, M.J., and Katz, I. “Potentials in a Plasma Over a Biased Pinhole”, IEEE Transactions in Nuclear Science, 1983, Vol. NS-30, No.6, p.4307-4310.

20. MIT Wavelength Tables, 1969, The M.I.T. Press, Cambridge, MA.

21. Stevens, N.J. “Space Environmental Interactions With Spacecraft Surfaces”, NASA TM 79016, January 1979.

22. Upschulte, B.L., Marinelli, W.J., Carleton, K.L., Weyl, G., Aifer, E., and Hastings, D.E. “Arcing on Negatively Biased Solar Cells in a Plasma Environment”, Journal of Spacecraft and Rockets, 1994, Vol.31, No.3, p.493-501.

23. NIST Atomic Spectra Database. URL:http://physics.nist.gov/cgi-bin/AtData

24. Anodic Coating For Aluminum and Aluminum Alloys, Mil. Specification, MIL-A-8625E, April 1988.

APPENDIX

Two examples of I-V curves that demonstrate the existence of two stable branches for the solution of the current balance equation.